Atmospheric
Measurement
Techniques

Developments on a 22 GHz microwave radiometer and reprocessing of 13-year time series for water vapour studies

Alistair Bell[1,2], **Eric Sauvageat**[1,2,a], **Gunter Stober**[1,2], **Klemens Hocke**[1,2], **and Axel Murk**[1,2]

[1]Institute of Applied Physics, University of Bern, Bern, Switzerland
[2]Oeschger Centre for Climate Change Research, University of Bern, Bern, Switzerland
[a]now at: Federal Office for Meteorology and Climatology MeteoSwiss, Payerne, Switzerland

Correspondence: Alistair Bell (alistair.bell@unibe.ch)

Abstract. Long-term observations of water vapour in the middle atmosphere are important for climate studies and predictions, chemical and dynamical process studies, and modelling certain weather events with implications for surface conditions. Measurements from an instrument making middle-atmosphere water vapour observations near Bern, Switzerland – named MIAWARA (MIddle Atmosphere WAter vapour RAdiometer) – have been completely reprocessed since 2010. This has comprised of a new calibration which has been integrated into the framework for the calibration of other University of Bern radiometers and a new retrieval algorithm. The installation of a new spectrometer on the instrument has also allowed the comparison and correction of past observations. We present these corrected measurements and their subsequent analysis against data from Aura's Microwave Limb Sounder (MLS). The comparison shows that the corrected spectra yield more consistent values of water vapour mixing ratio between MIAWARA and Aura MLS, with a lower standard deviation of differences at all heights and a reduced bias between the two instruments at pressure (height) levels below (above) 0.3 hPa.

1 Introduction

Changes in middle-atmosphere water vapour can result in important radiative forcings relevant to changes in global surface temperature (Solomon et al., 2010). Fluctuations will also affect temperatures in the middle atmosphere (Maycock et al., 2011) and can directly or indirectly affect the concentrations of other gases (Brasseur and Solomon, 2005; Thölix

et al., 2018). The mixing ratio of water vapour and horizontal and vertical gradients of water vapour are important for the circulations in the middle atmosphere, such as the Brewer–Dobson circulation, and changes in water vapour are commonly used as a tracer for such circulations (Straub et al., 2012; Hocke et al., 2018; Shi et al., 2023).

There are various methods for measuring water vapour in the atmosphere. In the troposphere, routine observations are often made using radiosondes like the RS-41 (Oyj, 2022). In the lower stratosphere, semi-routine measurements can be taken using in situ balloon-borne devices (Hurst et al., 2011; Graf et al., 2021; Brunamonti et al., 2023), although continuous monitoring in this region typically depends on remote sensing technologies (Sica and Haefele, 2016). In contrast, measuring water vapour in the upper stratosphere and mesosphere is more challenging due to the remoteness, extreme conditions, and the relatively low mass of water vapour in these layers. Due to these difficulties, microwave radiometry has become a common method for ground-based and satellite-borne instruments in these upper-atmospheric regions (Haefele et al., 2008; Straub et al., 2012; Schranz et al., 2019).

The Microwave Limb Sounder on board the Aura satellite, launched in 2004, remains a key source of global water vapour data for the middle atmosphere (Waters et al., 2006). However, the ageing of this and other long-operating instruments has led to measurement drifts, making it difficult to distinguish between real atmospheric changes and artefacts from the instruments themselves (Livesey et al., 2021). For instruments on board satellites, diagnosing and fixing instrumental problems can be difficult due to the remote nature of

the instrument. It is hence important to maintain a network of instruments, used with a collaborative approach, to ensure that data are reliable and to reduce the impact of individual instrument errors.

Although routine global measurements of water vapour in the middle atmosphere have been made with the microwave limb sounder on the Aura satellite since 2004, these observations face several drawbacks when compared to ground-based upward-looking radiometers. The Aura Microwave Limb Sounder (MLS) has a revisit time of twice per day at a fixed local time, meaning that observations can be sparse, and there is limited possibility of capturing diurnal variations. As satellite instruments cannot be serviced, instrumental ageing which can cause drifts in the measurements can be difficult to separate from atmospheric trends; thus it can be difficult to separate instrumental artefacts from measured values. The lifetime of a satellite is also finite; the satellite may fail due to aged electronics, fuel depletion or a range of other factors. The MLS instrument will end its lifetime in 2026, with the water vapour measurements severely restricted from spring 2024 (NASA Jet Propulsion Laboratory, 2024). Currently, there are no scheduled launches for a replacement instrument, which means that the most valuable resource for monitoring water vapour will be the network of ground-based radiometers.

2 MIAWARA

The MIddle Atmosphere WAter vapour RAdiometer (MIAWARA) is a 22 GHz radiometer that has been operated by the Institute of Applied Physics (IAP) at the University of Bern since April 2002 (Deuber et al., 2004). It was installed at the Zimmerwald Observatory near Bern in 2006 and has since provided long-term observations of this essential climate variable in the stratosphere and lower mesosphere.

The MIAWARA records the downwelling spectral radiance around the 22 GHz H_2O absorption line. This absorption line is a narrow range of frequencies across which radiation is increasingly absorbed by the air layer which it is passing through, and, through Kirchoff's law, it is increasingly emitted. As the intensity of this absorption line increases with the water vapour mixing ratio, surface radiance can be used to retrieve the water vapour mixing ratio. The effect of pressure broadening (Liebe, 1985) effectively increases the spectral width of emission with increasing atmospheric pressure. This allows the recorded spectral radiances to be inverted to retrieve vertical profiles of water vapour.

The instrument has a corrugated feed horn antenna which is directed towards a plane mirror. The mirror rotates, allowing a range of elevation angles and calibration targets to be observed, such as the reference target, hot load and liquid nitrogen target. As reflections between the receiver and external targets (notably the reference target) will cause unwanted standing wave errors, the mirror is mounted on a linear trans-

lation stage which alternates the distance from the horn antenna between the observations by a quarter wavelength. This changes the phase of the standing waves, and by averaging the data of the two positions the standing wave errors are reduced (Gustincic, 1977).

2.1 Calibration

As the 22 GHz line has a fairly small magnitude (of the order of 0.1 K), measurement noise and spectral non-linearities can severely affect the retrieved water vapour mixing ratio, the measurement response and the effective height range of the retrieval. In addition, the brightness temperatures observed in this frequency range, which are typically between 30 and 70 K at the zenith, are considerably lower than those of other frequently monitored microwave absorption lines, like the 183 GHz water vapour line, or those associated with ozone and oxygen.

In order to optimize the noise and linearity of the spectra, most middle-atmosphere water vapour radiometers use a scheme where the antenna view rapidly switches in quick succession between the sky (line view) and a reference (reference view) (Forkman et al., 2003). For this, the reference view produces a signal of around the same intensity as the line observation. For this radiometer, the sky view is at an angle that is calculated to optimize the middle-atmospheric emission whilst not being so low as to have excessive attenuation from the troposphere. This is an elevation angle that is typically between 15 and 30°, depending on the optical depth of the troposphere, which tends to be seasonally dependent. The reference observation is then the sky at zenith view partially blocked by a strip of the microwave absorber. The combination of the sky at zenith, which is cold compared to the observation at a lower elevation angle, and the absorber, which is at ambient temperature and much warmer than the observed sky radiances, means that a signal of around the same magnitude as the line observation can be made. The angle of the view is adjusted by up to 14°, allowing a variable contribution from the absorber to be contained in the antenna view, as less of the absorber is seen by the antenna at lower elevation angles.

Raw spectral measurements are represented in "counts", which are accumulated spectral values derived from the fast Fourier transform (FFT) of the time-domain signal sampled by the 8-bit ADC (analogue-to-digital converter). Since we accumulate data over several seconds, the quantization of these spectral counts is much finer than the original ADC resolution. In order to calibrate these measurements to the more useful unit of brightness temperature, hot and cold observations, with a known physical temperature are required. For this, a microwave absorber at ambient temperature is used for the hot target, and the sky at a high elevation angle is used for the cold target. The brightness temperature of the sky at this elevation angle is calculated by taking several further measurements at different elevation angles and perform-

ing a tipping curve calibration (Han and Westwater, 2000). This tipping curve measurement is currently performed once every 15 min and contains seven different elevation angles, though the number of angles, the period between successive tipping curves and integration time at each observation angle have been changed slightly over the years.

The difference between the line and reference counts is calibrated with the differences in hot and cold temperature and hot and cold counts according to Eq. (1). This brightness temperature difference is then corrected for tropospheric attenuation by a factor calculated from the tropospheric optical depth calculated previously.

$$\Delta T_b = \frac{(U_{Line} - U_{Ref})}{(U_{Hot} - U_{Cold})} \cdot (T_{Hot} - T_{Cold}) \tag{1}$$

From Ingold et al. (1998), the downwelling brightness temperature at the tropopause can be estimated by modelling the atmosphere as a two-layer system. Although in the calibration the emission from the troposphere is not corrected for – as this is easily corrected for in the retrieval step – the attenuation of the signal coming from middle-atmospheric emissions through the troposphere is corrected for. This step allows the retrieval to assume an instrument altitude above the tropopause, meaning that the troposphere does not need to be taken into account in the radiative transfer model.

A correction factor a, which corrects for the tropospheric absorption based on the previously calculated optical depth, can be applied. The formula also corrects for the relative air masses of the troposphere and middle atmosphere viewed by the reference observation (AM_{ref_trop} and AM_{ref_ma}) and the line observation (AM_{line_trop} and AM_{line_ma}). The product of the correction factor and the brightness temperature difference then gives a brightness temperature difference equivalent to a zenith angle view (i.e. with an air mass factor of 1).

$$a = \frac{1}{\begin{array}{c}AM_{line\_ma} \cdot \exp\left(-\tau \cdot AM_{line\_trop}\right) \\ -A \cdot AM_{ref\_ma} \cdot \exp\left(-\tau \cdot AM_{ref\_trop}\right)\end{array}} \tag{2}$$

$$T_{b_{Bal}} = a \cdot \Delta T_b \tag{3}$$

Among other weather conditions that can lead to increased noise in the spectra, precipitation has the greatest impact. When the presence of precipitation is sensed by a rain sensor, the rain hood on the instrument closes. Although the instrument still runs, there is now a rain-covered radome between the sky and the antenna, adding effects of attenuation and reflection to the measurements. As readings containing rainy data tend to increase the noise of a spectrum for a given day, all readings taken when the rain hood is closed are excluded from the calibrations.

For the reprocessed dataset, it was found that an optimal integration time of 1 d would be used for retrievals. This is

a compromise between having a good enough temporal resolution to resolve changes with time and having low enough noise in the calibrated spectra so that a retrieved profile with a large enough height range could be made.

2.2 Retrieval

The retrieval of the water vapour profile from the calibrated spectra is handled by the radiative transfer software ARTS (Buehler et al., 2018), which is integrated into the MATLAB software Qpack (Buehler et al., 2018). The Levenberg–Marquardt algorithm calculates updates of the water vapour state x upon each new iteration within the algorithm.

The retrieval of water vapour in the middle atmosphere relies on a high spectral resolution, and as such, across a 1 GHz bandwidth, brightness temperatures at several thousand frequencies are calibrated (see Table 1). In order to compute the forward model with such a large number of frequencies, which is calculated at each iteration of the optimal estimation algorithm, a non-trivial amount of computational power is required. In order to speed up retrieval time, the forward model is run at the frequency resolution of the instrument at the central frequency, and then the spacing between the channels is increased with distance from the 22.235 GHz absorption line frequency so that only 1200 frequencies are simulated altogether.

For the optimal estimation approach (Rodgers, 2000), a first guess or a priori value is needed. This is what can be considered the best estimate of the retrieval state x, which in this case is a vertical profile of the water vapour mixing ratio. In this case, two sources of information were chosen for the a priori profile: the ECMWF analysis of 6 years (2010–2015) was used. The average zonal monthly mixing ratios were computed from this.

As the height range of this forecast only extends as far as 0.024 hPa, the MLS dataset (see Sect. 3.4) is also used for heights above 0.5 hPa. The two profiles are used between 0.5 and 0.024 hPa, over which pressures a cubic smoothing spline function is applied (MATLAB function `csaps` based on De Boor, 1978). To compute values for a specific date, an interpolation of the average monthly zonal H_2O from the 2 nearest months to that date (e.g., averages from April and May for a date of 30 April) is performed, considering their distances from the target date.

Another important source of error comes from the estimation of the a priori error covariance matrix. For the retrieval framework here, a full matrix is not prescribed; however, a profile of estimated standard deviations along with a correlation length of 0.25 is provided. An estimation of the a priori state for each month was performed by calculating the standard deviation of water vapour above Bern measured on the first day of each month between 2010 and 2018. As shown in Fig. 1, despite some differences between months at different levels, there were no significant seasonal differences. Because of this, a static profile of standard deviations is used

Table 1. Specifications of the main spectrometers used on board the MIAWARA instrument.

	Chirp transform	AOS	AC-240	USRP
Manufacturer	Paul Hartogh (MPS) and University of Bern	Observatoire de Meudon	Acqiris	Ettus Research
Bandwidth	40 MHz	1.1 GHz	1 GHz	2×200 MHz
No. channels	4200	1725	16 384	$2 \times 16\,384$
Channel spacing	9.5 kHz	610 kHz	61 kHz	12.2 kHz
Frequency resolution	14.07 kHz	1.1 MHz	61 kHz	12.2 kHz
Reference	Hartogh (1997)	Jost et al. (1996)	Benz et al. (2005)	Hagen et al. (2020)

to generate the a priori error covariance matrix, generated from the average standard deviations from all 12 months. In order to generate a more continuous profile from the calculated standard deviations, additional points are added to the vertical axis, and interpolation is performed using the SciPy `interp1` function with a cubic smoothing function (Virtanen et al., 2020). This is further smoothed by convolving the profile with a Gaussian kernel to reduce the remaining oscillations. Before being used in the retrieval algorithm, the profile is further increased by 0.2 ppmv at each level to account for resolution and/or grid spacing errors and integration time differences which are not accounted for in the yearly variability. An extra requirement is made of the a priori standard deviations, which is that they are between 20 % and 80 % of the a priori profile at any given level. Should the errors fall outside of this range, they are increased or decreased until they are in agreement with it.

The correction for the tropospheric attenuation of the middle-atmospheric signal allows the retrieval surface height to be set at 15 km. A bandwidth of only 70 MHz is used for the retrieval, as bandwidths larger than this, whilst improving the effective range of the retrievals, were seen to cause additional problems in managing the spectral baselines (such as in Nedoluha et al., 2013; Verdes et al., 2002) and could often lead to degraded retrievals. To account for any mismatch in the frequency axis, a frequency shift is retrieved. The spectral baseline, which is often seen in the calibrated spectra, is a major problem which limits both the height range and the accuracy of retrievals. This is a known problem and can come from numerous sources, such as the standing waves discussed in Sect. 2. For several reasons, the shift in mirror position is not able to completely remove such artefacts. This can be due to the change in path length meaning that different views of the reference bar are seen with the different positions, as well as several other reasons which are discussed in great detail in Deuber and Kämpfer (2004).

In addition, although the tropospheric attenuation affecting the signal from the middle atmosphere is accounted for in the calibration step, the emission from the troposphere is not corrected for. This means that the balanced brightness temperature contains a baseline contribution from the tropospheric emission. In order to remove this baseline, a second-degree polynomial fit is retrieved inside the optimal estimation algorithm.

The spectral baseline which affects measurements may be irregular, be non-symmetric and change over time, all of which make it difficult to systematically remove. Although a common approach to this problem is to try to fit sinusoidal functions to the brightness temperature spectra, such as by Sauvageat et al. (2022), an issue with this approach in this instance was "over-fitting". This can happen when there are features in the spectra that could be fitted by a sinusoidal function over a given frequency range but not over all the spectra. This can then have the effect of creating features in the spectra, which in the optimal estimation can create something non-physical in the retrieved profile.

2.3 Updates

Several hardware upgrades have been made to the instrument since its first observations in 2001. The most notable of these has been to the spectrometer. The spectrometer is a key component of the receiver, which converts the time-domain electrical signal into a frequency-domain signal. The working bandwidth, frequency resolution and linearity of the spectrometer have large implications for the quality of the water vapour profile that can be retrieved.

As developments in spectrometer hardware have been made over the lifetime of MIAWARA, the spectrometers have been updated. As the instrument has been designed to accommodate up to three spectrometers, this allows an intercomparison of the calibrated spectra and brightness temperatures to be made between spectrometers.

Originally, two spectrometers were installed on the instrument (Deuber et al., 2004): an acousto-optical spectrometer (AOS) for broadband analysis and a chirp transform spectrometer with 4200 channels for the precise analysis of the line centre. Technological advances from FFT spectrometers have been shown to provide significant improvements over AOSs and filter bank spectrometers in terms of resolution, bandwidth and system stability (Muller et al., 2009). For this reason, a broadband FFT spectrometer, the Acqiris AC-240, was also installed on the instrument in 2007 and is due to record measurements until at least the end of 2024. However, the Acqiris AC-240 has recently been shown to have issues
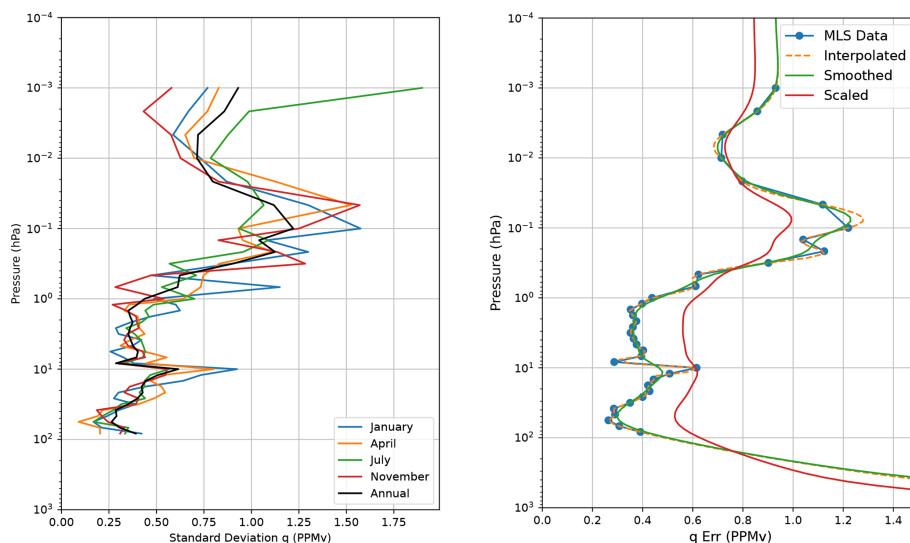
Figure 1. Standard deviation across pressure levels found from MLS data, and the yearly, smoothed data used to generate the error covariance matrix in the retrieval algorithm.

with non-linearity (Sauvageat et al., 2021), which is examined in this article in Sect. 3. In November 2022, a new FFT spectrometer was installed, based on the software-defined radio (SDR) universal software radio peripheral (USRP) X310 manufactured by Ettus Research (Hagen et al., 2020). It has two input receivers, which can be tuned over a frequency range from 10 MHz to 6 GHz. Both channels have a usable bandwidth of slightly under 200 MHz, giving a 12.2 kHz channel spacing. The spectrometer demonstrates reduced bias and improved linearity compared to the AC-240. This improvement could stem from the 14-bit analogue-to-digital converter (ADC), a notable step up from the AC-240's 8-bit ADC, as well as advancements in digital signal processing that reduce numerical errors. The main features of each spectrometer is summarized in Table 1.

2.4 Reprocessing

The raw spectra obtained from the instrument have been reprocessed from October 2010 until October 2023, which is shown in Fig. 2. The new calibration routine has been integrated into a unified calibration framework for radiometers managed by the University of Bern (Sauvageat, 2021). Importantly, additional quality checks have been added to the calibration cycle (e.g. noise in spectra too high, median brightness temperature outside of 3 standard deviations of other median brightness temperatures in integration time, mean balanced brightness temperature being lower than -5 K or higher than 5 K). Where these quality checks are not passed, the spectra are not included in the integrated measurement.

Although in the past variable integration times have been used based on the spectral noise (Lainer et al., 2018), for the reprocessed data it has been considered more useful to have

a dataset with a consistent temporal resolution. For this reason, the level 1b data (calibrated, integrated data with quality checks) have been processed and integrated into a temporal resolution of one spectrum per day. It was found that with integration times of less than 1 d, on days with less than optimal observing conditions, the spectral noise could noticeably affect the retrieval range. Conversely, integration times of more than 1 d did not lead to a significant improvement in retrieval quality whilst limiting the usefulness of such a dataset.

3 Comparative performance of AC-240 and USRP spectrometers

The USRP spectrometer was installed on the instrument in November 2022. At the same time, a number of maintenance tasks, such as the replacement of the reference bar absorber, were also performed. Although the spectrometer provided measurements for the first few days after installation, in November there was a software problem that led to the spectrometer not recording observations again until the start of 2023.

3.1 Calibrated spectra

In order to verify the new spectrometer, the calibrated spectra from the two were compared for a liquid nitrogen (LN2) calibration made in March 2022. During the LN2 calibration, observations were taken of the hot load, LN2 target, cold sky, and reference and line views, which allowed a calibration of the line and reference views that is independent of the tipping curve calibration. Figure 3 shows the calibrated line and reference observations measured on the two spectrometers, where line observations are shown in blue and the reference
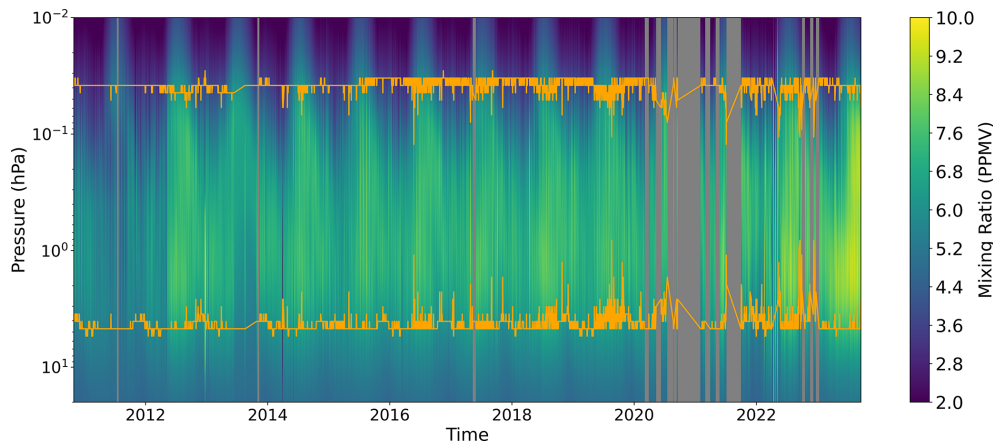
Figure 2. Reprocessed MIAWARA time series from October 2010 until October 2023, all made with the AC-240 spectrometer (right). The area between the two orange lines indicates where the measurements have a measurement response above 0.6, meaning that most of the information comes from the atmospheric signal and not the a priori signal. The grey areas show where there were no measurements made of acceptable quality for more than 5 consecutive days.

in red. One can see from this image that the reference observation is not exactly that which one would expect from the theory presented. Instead, there seems to be a sinusoidal oscillation in the spectra between 21.7 and 22.1 GHz, after which there is a linear decrease in brightness temperature up to around 22.5 GHz. This is likely due to the frequency dependency of the antenna pattern, causing a larger proportion of the hot absorber to be seen at some frequency ranges compared to others.

It may be seen that, despite the vertical shift in the spectra by around 0.1 K for the reference observation and 0.2 K for the line observation, the spectra agree in shape fairly well. The differences between the measurements recorded on the USRP and AC-240 were then computed, binning the USRP measurements by 50 frequency vectors and the AC-240 by 10 frequency vectors. When the differences between the spectra are computed for each frequency, some features become more evident. For example, there is a feature that is clear on both the line and reference measurements at a frequency offset of -25 and 25 MHz, where there appears to be a slight oscillation. This is caused by the non-linearity of the AC-240 spectrometer and is visible if one looks closely at the line and reference spectra. Though this feature cannot be considered to be ideal, as it appears in the reference and the line observation, and the difference between these spectra is used for the retrieval of water vapour, the feature is cancelled out, and the brightness temperatures in this frequency range may be safely used in the retrieval algorithm.

It may also be seen in this figure that at the line centre, there is a decrease in the bias. This is most likely caused by the central two channels of the AC-240 that do not give accurate readings (Gomez et al., 2012). In the updated retrieval framework, these two central frequencies are not used. Though the non-linearities present in the AC-240 spectrom-

eter are evident from this comparison, a further known bias, due to spectral leakage (Sauvageat et al., 2021), is not evident. This was potentially due to the relatively large noise levels in these calibrations due to the short integration times of several hours compared to the operational integration time of 1 d.

In order to compare the two spectrometers with a minimized noise level, 1 year of calibrated balanced brightness temperature measurements was used between the installation of the spectrometer in November 2022 and October 2023. Due to several software issues, the USRP did not make readings for the whole time period, and thus a dataset of 265 d during which measurements were made with both spectrometers was used. Readings for which one of the spectrometers contained readings outside of 3 standard deviations for more than 5 % of the spectra were discarded. With the rest of the data, the median brightness temperature at each frequency on each spectrometer was computed. The differences between the two spectrometers was then found. This result is shown in Fig. 4. One can see in this figure that the USRP records throughout the frequency range larger values than the AC-240. It can also be seen that the features of the calibrated spectra are clear in this plot of the differences between spectrometers, indicating that the bias is proportional to the brightness temperature itself. According to the methodology presented in Sauvageat et al. (2021), the effects of spectral leakage may be corrected for by using Eq. (4):

$$T_{\mathrm{B,corr}} = \frac{1}{(1-\alpha)} \left(T_{\mathrm{B}} - \overline{T}_{\mathrm{B}} - \Delta T_{\mathrm{B,c}} \right), \qquad (4)$$

where $T_{\mathrm{B,corr}}$ is the brightness temperature corrected for the effects of spectral leakage, α is the scaling factor, $\overline{T}_{\mathrm{B}}$ is the mean brightness temperature from a single measurement across all frequencies, and $\Delta T_{\mathrm{B,c}}$ is a non-linearity correction. The non-linearity correction is an additional correction
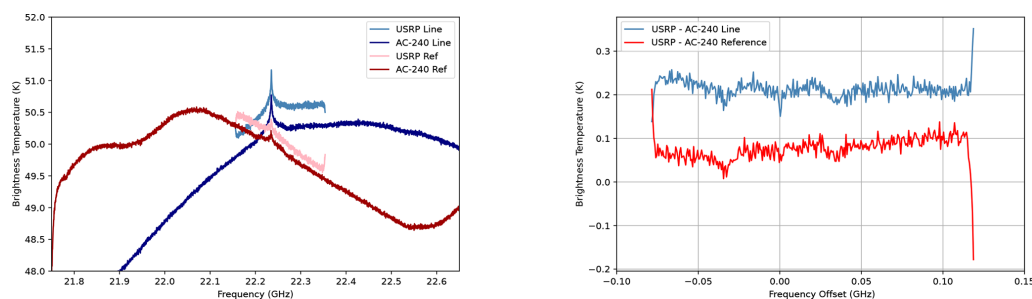
Figure 3. Measurements of the line and reference observation views calibrated with an LN2 calibration taken as recorded on the AC-240 and USRP spectrometers (left) and the difference between the two spectrometers for two observation views (right).
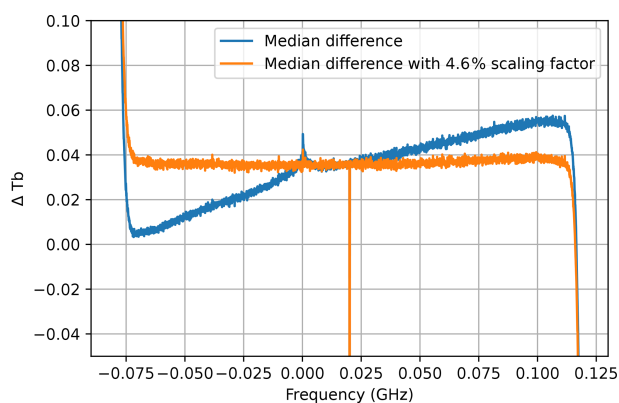

Figure 4. The differences in balanced brightness temperature between measurements by the USRP spectrometer and the AC-240 (USRP − AC-240), as well as the USRP and the AC-240 when a scaling factor of 4.6 % is applied to the spectra.

based on the absolute brightness temperature and was found to amount to a maximum of around 0.2 K for a brightness temperature increase of 100 K. As this is a relatively minor amount for the range of calibrated brightness temperatures used in the retrievals, which tend to have a range on the order of 1 K, the non-linearity term here was not considered. When the AC-240 was scaled by 4.6 %, both the slope and the line feature are removed. This indicates that the problem of spectral leakage is present in the AC-240 and that it could be corrected for by a 4.6 % scaling factor.

3.2 Retrieval range and resolution

One key advantage of the USRP over the AC-240 in making retrievals of middle-atmosphere water vapour is the spectral resolution, which is 5 times higher than the AC-240 (see Table 1). A higher spectral resolution could in theory allow a larger retrieval range, as the centre of the absorption line, from which information about the water vapour mixing ratio higher up in the atmosphere comes, is better resolved. One way of judging the information content by height can be gained by looking at the averaging kernel from the retrieval. The averaging kernel represents the sensitivity of the

retrieved state to changes in the true state. An ideal averaging kernel would therefore be an identity matrix. However, as information is spread across many retrieval levels, this is not the case.

From the plots of the two averaging kernels, shown in Fig. 5, one can see that similar values are found at the maximum sensitivity of averaging kernels up to around 0.04 hPa. Above the height corresponding to this pressure level, retrievals from the USRP spectrometer have a higher sensitivity than those from the AC-240, although the sensitivity is around half that found between 1 and 0.1 hPa. The averaging kernels at pressures below 0.02 hPa also seem to have a bimodal distribution and a certain skewness.

The value of the averaging kernel at maximum sensitivity gives information about the validity of the retrieval level at which this occurs, and the full width at half maximum (FWHM) for each retrieval level can also be of interest. If the maximum of a column is located along the diagonal, it indicates that the retrieved level has the highest sensitivity to its corresponding true level. This is a good sign as it means the retrieval is most sensitive to the actual level that it is supposed to represent. The wider the FWHM, the wider the information is spread among the retrieved states and hence the lower the vertical resolution of the retrieval.

Figure 6 shows that between 2 and 0.08 hPa, the averaging kernel for both the AC-240 and the USRP is centred very close to the retrieval pressure level, as desired. At lower pressures, retrievals from both spectrometers have the maximum sensitivity at pressure levels below the retrieval level. However, the retrieval level from the USRP measurements stays within the FWHM up to 0.004 hPa, whereas for the AC-240, the FWHM stays within the retrieval level pressure only up to 0.020 hPa, although it must be highlighted that, as shown in Fig. 5, the sensitivity at these higher levels is approximately a third of that at 1 hPa. The FWHM between 1 and 0.1 hPa is slightly improved with the USRP, which is demonstrated with the smaller error bars. From these findings, it would be expected that retrievals with the new spectrometer would be more representative than retrievals made with the AC-240 spectrometer for water vapour deviations from the a priori profile above 0.1 hPa.
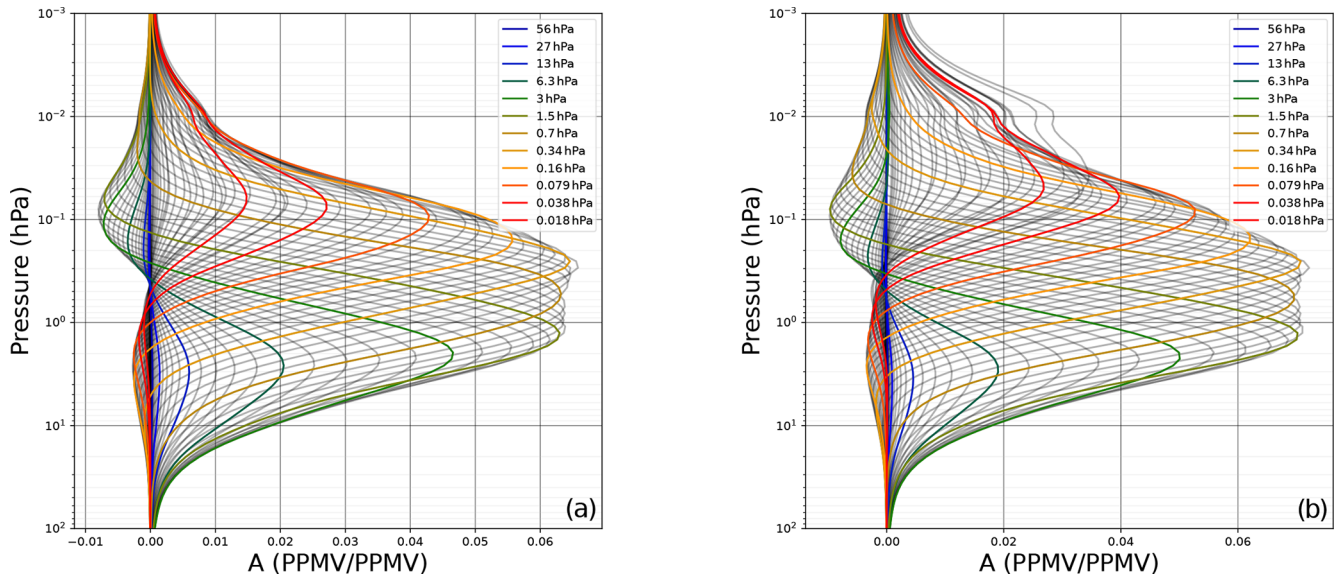
Figure 5. Mean averaging kernel for retrievals made with the AC-240 **(a)** and USRP **(b)** spectrometers between November 2022 and October 2023.
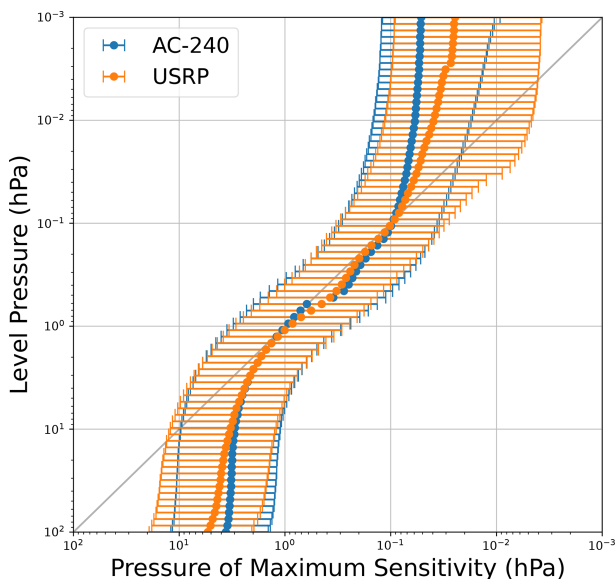

Figure 6. Pressure of maximum sensitivity of the retrieval to changes in the true state, with the error bars representing the pressure at which the curve is equal to half the maximum value.

3.3 Retrieved water vapour

The differences in the averaging kernel of the retrieval and differing spectrometer properties will impact the values of retrieved water vapour. As the retrieval is handled by virtually the same algorithm for measurements made by both spectrometers, save for some adaptions to the instrumental errors to take into account different frequency resolutions, retrievals from observations made with both spectrometers in parallel

can be directly compared and differences directly attributed to the hardware difference.

As shown in Fig. 7, there is a bias of below 1 ppmv in the profiles retrieved with the AC-240 relative to those retrieved with the USRP between 1 and 0.1 hPa that persists between the start and end of the period. The AC-240 also contains a negative bias in spring at pressures around 0.01 hPa, whilst in the summer this bias fades and is replaced by a negative bias at pressures around 4 hPa.

Despite the fact that the differences between the two spectrometers appear to be significant, by comparing the distribution of retrieved values to the a priori climatology, it may be seen that the differences between retrieved profiles are relatively small compared to the differences between retrieval and climatology. This is influenced by the fact that 2022 and 2023 have been marked by significantly higher levels of water vapour in the stratosphere and mesosphere compared to the average (Millan et al., 2022; Nedoluha et al., 2023; Zhou et al., 2024). In fact the median values agree very well up to 1 hPa, above which they diverge slightly to have a maximum difference in median mixing ratio of 0.62 ppmv at 0.34 hPa.

Comparing the differences in retrieved water vapour from the non-scaled AC-240 measurements and the scaled AC-240 measurements can show whether the retrieved values become more consistent with those from the USRP and not simply that the median retrieval is more similar to that of the USRP. In Fig. 8, the distribution of the differences between the unscaled AC-240 retrievals and the USRP retrievals, as well as the scaled AC-240 retrievals and the USRP retrievals, is presented, all at four pressure levels between 0.1 and 1 hPa.
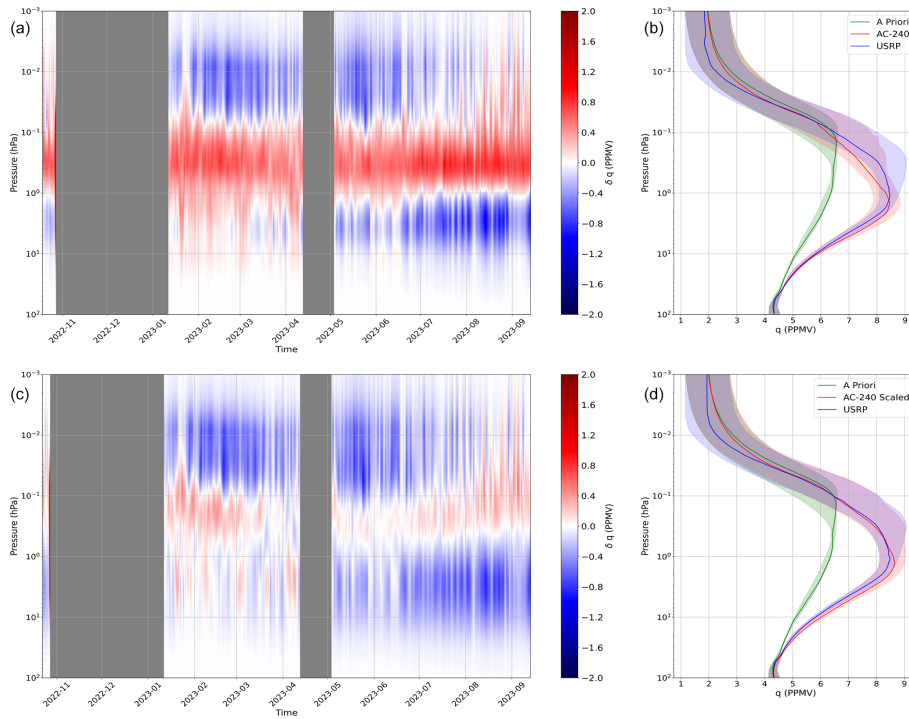
Figure 7. The difference between profiles of water vapour measured with the USRP and the AC-240 spectrometer (USRP − AC-240), between the installation date in November 2022 and October 2023 **(a)**, and the median with 25th and 75th percentiles (translucent) of the a priori profile, retrieved values from AC-240 measurements, and retrieved values from USRP measurements **(b)**. The same plots are shown again in panels **(c)** and **(d)** but for AC-240 measurements that are corrected with the scaling factor.
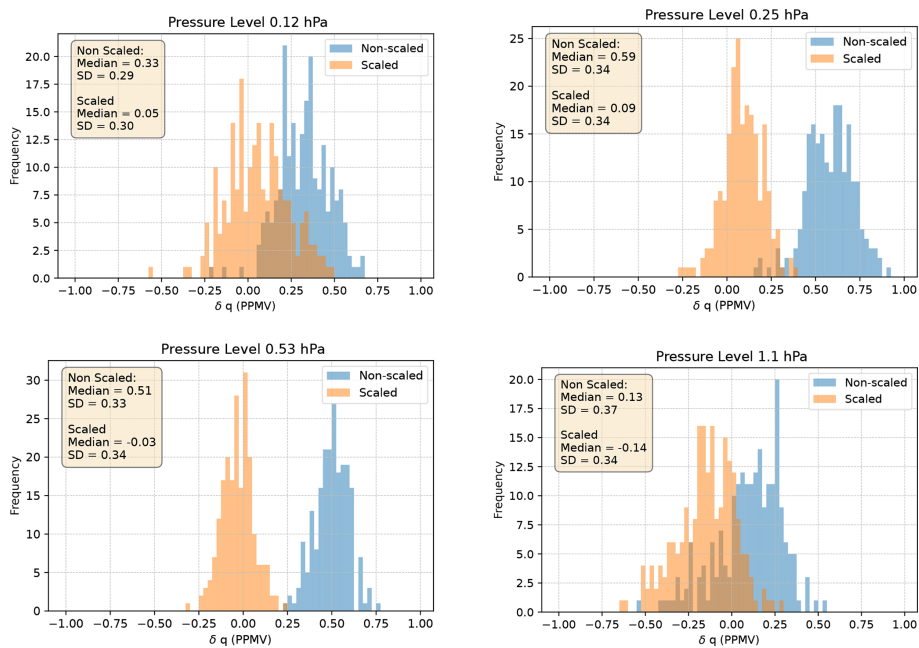
Figure 8. Histograms of the difference in the retrieved water vapour with USRP minus AC-240, where AC-240 retrievals with the corrected measurements, made with a 4.6 % scaling factor, are compared to the uncorrected measurements. These are shown at pressure levels indicated in the title of each panel.

3.4 Comparison to MLS

The Microwave Limb Sounder (MLS) on board the Aura satellite is a microwave radiometer containing five receivers with a total of 1308 frequency channels, which allow the retrieval of at least 15 atmospheric constituents, plus temperature profiles, at height ranges varying by species from up to 80 km down to 5 km (Waters et al., 2006). Due to the frequency of measurements and the possibility of co-located measurements, MLS is often used as a reference to compare other middle-atmosphere measurements to. Despite this, MLS observations have been subject to an instrumental drift, which, though corrected for in version five (V5) of the measurement dataset, still has a drift when compared to frost point hygrometers. They do, however now exhibit no drift when compared to the Atmospheric Chemistry Experiment Fourier transform spectrometer (ACE-FTS) (Livesey et al., 2021).

In order to verify the reprocessed retrieval and whether the re-scaled calibrated spectra agree better with other measurements of middle-atmosphere water vapour, MLS was thus used for comparison. From Livesey et al. (2022), due to the high vertical resolution of MLS measurements compared to other remotely sensed observations, it is common to compare measurements without reference to the MLS averaging kernel. This was the approach that was taken in this work, and to compare MIAWARA measurements to MLS, the MLS profile was convolved with the MIAWARA averaging kernel. An 8-year dataset from January 2015 until October 2023 was created, for which period both MLS observations and MIAWARA observations were available.

Figure 10 shows the differences between the MLS and MIAWARA measurements from the period between 2015 and 2023. There appears to be an annual pattern to the differences in retrievals, with biases becoming greater in the summer period compared to the winter. This pattern is the same for both the uncorrected and corrected AC-240 spectra. It can also be seen that the negative bias, between 10 and 1 hPa from 2022 until the end of the period, becomes greater, coinciding with above-average water vapour mixing ratios seen throughout this period. A similar effect is seen in the ozone radiometer SOMORA (Sauvageat et al., 2022) and has been hypothesized to come from a seasonal-dependent baseline or due to changes in the optical depth of the troposphere in summer compared to winter. As the tropospheric optical depth is also used to correct for the attenuation of middle-atmosphere water vapour absorption line signal (see Sect. 2.1), it is possible that errors in the calculation of the optical depth which increase in summer could result in the pattern seen in Fig. 10. When the MLS differences with the uncorrected spectra and the corrected spectra are compared, it can be seen that the positive bias between 0.1 and 0.2 hPa is less intense with the corrected spectra, whilst the negative bias is slightly increased.
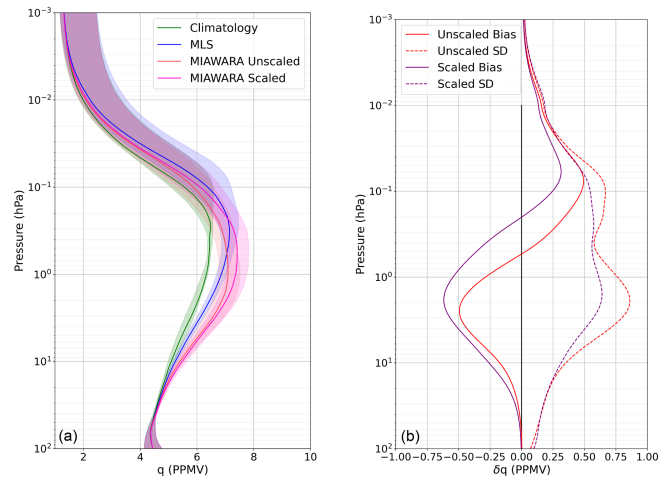

Figure 9. Median water vapour profiles from measurements provided by MLS: the uncorrected AC-240 spectra and the corrected AC-240 spectra **(a)**. The 25th to 75th percentiles are shown in translucent shading of the corresponding colour. The bias and standard deviation (MLS − MIAWARA) of the difference between the MLS measurement and the uncorrected and corrected AC-240 measurements **(b)**.
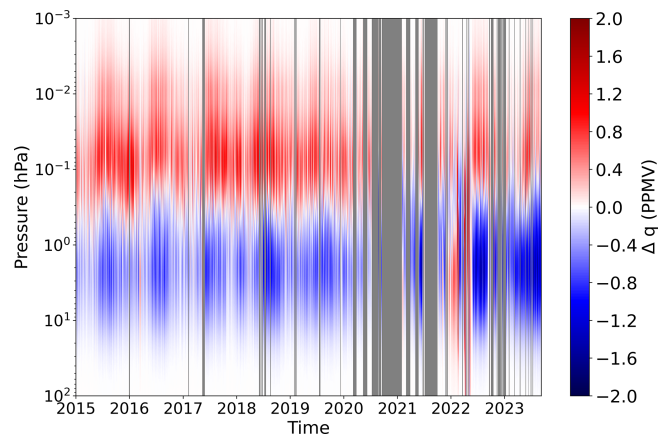

Figure 10. Time series of the difference between MLS water vapour and MIAWARA measurements made with the corrected spectra.

Figure 9 shows that the MIAWARA estimates a higher water vapour mixing ratio than the MLS between 10 and 0.2 hPa and that the profile maximum occurs slightly lower in altitude on the MIAWARA than the MLS. Although the bias in the retrieved water vapour with the corrected spectra is slightly degraded below 0.3 hPa relative to MLS, the inverse is true above this pressure level. The standard deviation of differences is also improved relative to the uncorrected differences, indicating that changes in water vapour are more consistent between MLS and the corrected measurements compared to the uncorrected measurements.

4 Conclusions

An overview of a key upgrade to the MIAWARA instrument, the installation of a new spectrometer, has been presented, alongside analysis of the calibrated spectra and the effect on retrievals with this new spectrometer. A key finding was the need for a scaling correction of 4.6 % to the calibrated spectra of the AC-240 spectrometer which has been recording measurements on the MIAWARA instrument for the past 13 years and more.

The dataset presented is of use both in detecting water vapour trends in the middle atmosphere and in providing another valuable reference to other instruments capable of measuring water vapour in the middle atmosphere, such as the MLS and the ACE-FTS.

The result of a scaling factor of 4.6 % was notably smaller than the scaling factor needed to correct the spectra in the work of Sauvageat et al. (2021), who found that an 8 % scaling factor was able to correct for the effects of spectral leakage in their experiment. It is also less than the value of 7 % documented in Nedoluha et al. (2022). For the analysis presented here, the 4.6 % scaling factor seems to both bring the retrieved water vapour profile closer to the profiles retrieved from the USRP measurements and improve the retrievals with respect to the Aura MLS measurements. Both these results indicate that this correction improves the accuracy of MIAWARA water vapour measurements.

As highlighted briefly in the earlier comparison of the USRP and AC-240 spectrometers, the years 2022 and 2023 have been quite an exception in terms of the water vapour anomaly. This has arisen in the aftermath of the 2022 Hunga Tonga–Hunga Ha'apai volcano which emitted a plume posited to have reached up to the mesosphere (Nedoluha et al., 2024). The observations from the MIAWARA, alongside other datasets, will be used to analyse the impact of the volcano on middle-atmospheric water vapour and the possible impacts this has had. The MIAWARA dataset will also be used for the calculation of trends and monitoring of middle-atmosphere water vapour.

The instrumental upgrade presented, combined with the unique environmental conditions following the 2022 Hunga Tonga–Hunga Ha'apai volcanic eruption, presents an opportunity to develop a deeper understanding of atmospheric dynamics and the influences of major geophysical events on water vapour distributions in the middle atmosphere.

References

Bell, A.: Retrieved Water Vapour Profiles from MIAWARA at the Zimmerwald Observatory, Bern, Switzerland, NDACC/EVDC – ESA Atmospheric Validation Data Centre [data set], https://doi.org/10.60897/pdyc-8v84, 2023.

Bell, A.: alistairbbell/devs_22ghz_radiometer: Article analysis, Zenodo [code], https://doi.org/10.5281/zenodo.14608688, 2025.

Benz, A. O., Grigis, P. C., Hungerbühler, V., Meyer, H., Monstein, C., Stuber, B., and Zardet, D.: A broadband FFT spectrometer for radio and millimeter astronomy, Astron. Astrophys., 442, 767–773, 2005.

Brasseur, G. P. and Solomon, S.: Aeronomy of the middle atmosphere: Chemistry and physics of the stratosphere and mesosphere, Vol. 32, Springer Science & Business Media, https://doi.org/10.1007/1-4020-3824-0, 2005.

Brunamonti, S., Graf, M., Bühlmann, T., Pascale, C., Ilak, I., Emmenegger, L., and Tuzson, B.: SI-traceable validation of a laser spectrometer for balloon-borne measurements of water vapor in the upper atmosphere, Atmos. Meas. Tech., 16, 4391–4407, https://doi.org/10.5194/amt-16-4391-2023, 2023.

Buehler, S. A., Mendrok, J., Eriksson, P., Perrin, A., Larsson, R., and Lemke, O.: ARTS, the Atmospheric Radiative Transfer Simulator – version 2.2, the planetary toolbox edition, Geosci. Model Dev., 11, 1537–1556, https://doi.org/10.5194/gmd-11-1537-2018, 2018.

De Boor, C.: A practical guide to splines, Vol. 27, Springer-verlag New York, ISBN: 978-0-387-95366-3, 1978.

Deuber, B. and Kämpfer, N.: Minimized standing waves in microwave radiometer balancing calibration, Radio Sci., 39, 1–8, 2004.

Deuber, B., Kampfer, N., and Feist, D. G.: A new 22-GHz radiometer for middle atmospheric water vapor profile measurements, IEEE T. Geosci. Remote, 42, 974–984, 2004.

Forkman, P., Eriksson, P., and Winnberg, A.: The 22 GHz radio-aeronomy receiver at onsala space observatory, J. Quant. Spectrosc. Ra., 77, 23–42, 2003.

Gomez, R. M., Nedoluha, G. E., Neal, H. L., and McDermid, I. S.: The fourth-generation water vapor millimeter-wave spectrometer, Radio Sci., 47, 1–11, 2012.

Graf, M., Scheidegger, P., Kupferschmid, A., Looser, H., Peter, T., Dirksen, R., Emmenegger, L., and Tuzson, B.: Compact and lightweight mid-infrared laser spectrometer for balloon-borne water vapor measurements in the UTLS, Atmos. Meas. Tech., 14, 1365–1378, https://doi.org/10.5194/amt-14-1365-2021, 2021.

Gustincic, J.: A quasi-optical receiver design, in: 1977 IEEE MTT-S International Microwave Symposium Digest, San Diego, California, USA, IEEE, 99–102, 1977.

Haefele, A., Hocke, K., Kämpfer, N., Keckhut, P., Marchand, M., Bekki, S., Morel, B., Egorova, T., and Rozanov, E.: Diurnal changes in middle atmospheric H_2O and O_3: Observations in the Alpine region and climate models, J. Geophys. Res.-Atmos., 113, D17303, https://doi.org/10.1029/2008JD009892, 2008.

Hagen, J., Luder, A., Murk, A., and Kämpfer, N.: Frequency-Agile FFT Spectrometer for Microwave Remote Sensing Applications, Atmosphere, 11, 490, https://doi.org/10.3390/atmos11050490, 2020.

Han, Y. and Westwater, E. R.: Analysis and improvement of tipping calibration for ground-based microwave radiometers, IEEE T. Geosci. Remote, 38, 1260–1276, 2000.

Hartogh, P.: High-resolution chirp transform spectrometer for middle atmospheric microwave sounding, in: Satellite Remote Sensing of Clouds and the Atmosphere II, SPIE, 3220, 115–124, 1997.

Hocke, K., Lainer, M., Bernet, L., and Kämpfer, N.: Mesospheric inversion layers at mid-latitudes and coincident changes of ozone, water vapour and horizontal wind in the Middle Atmosphere, Atmosphere, 9, 171, https://doi.org/10.3390/atmos9050171, 2018.

Hurst, D. F., Oltmans, S. J., Vömel, H., Rosenlof, K. H., Davis, S. M., Ray, E. A., Hall, E. G., and Jordan, A. F.: Stratospheric water vapor trends over Boulder, Colorado: Analysis of the 30 year Boulder record, J. Geophys. Res.-Atmos., 116, D02306, https://doi.org/10.1029/2010JD015065, 2011.

Ingold, T., Peter, R., and Kämpfer, N.: Weighted mean tropospheric temperature and transmittance determination at millimeter-wave frequencies for ground-based applications, Radio Sci., 33, 905–918, 1998.

Jost, H., Kampfer, N., Lecacheux, A., and Rosolen, C.: Broadband acoustooptic spectrometer used as backend for remote sensing

of trace gases in the atmosphere, IEEE T. Geosci. Remote, 34, 927–935, 1996.

Lambert, A., Read, W., and Livesey, N.: MLS/Aura Level 2 Water Vapor (H2O) Mixing Ratio V005, Goddard Earth Sciences Data and Information Services Center (GES DISC) [data set], Greenbelt, MD, USA, https://doi.org/10.5067/Aura/MLS/DATA2508, 2020.

Lainer, M., Hocke, K., and Kämpfer, N.: Long-term observation of midlatitude quasi 2-day waves by a water vapor radiometer, Atmos. Chem. Phys., 18, 12061–12074, https://doi.org/10.5194/acp-18-12061-2018, 2018.

Liebe, H. J.: An updated model for millimeter wave propagation in moist air, Radio Sci., 20, 1069–1089, https://doi.org/10.1029/RS020i005p01069, 1985.

Livesey, N. J., Read, W. G., Froidevaux, L., Lambert, A., Santee, M. L., Schwartz, M. J., Millán, L. F., Jarnot, R. F., Wagner, P. A., Hurst, D. F., Walker, K. A., Sheese, P. E., and Nedoluha, G. E.: Investigation and amelioration of long-term instrumental drifts in water vapor and nitrous oxide measurements from the Aura Microwave Limb Sounder (MLS) and their implications for studies of variability and trends, Atmos. Chem. Phys., 21, 15409–15430, https://doi.org/10.5194/acp-21-15409-2021, 2021.

Livesey, N. J., Read, W. G., Wagner, P. A., Froidevaux, L., Santee, M. L., Schwartz, M. J., Lambert, A., Valle, L. F. M., Pumphrey, H. C., Manney, G. L., Fuller, R. A., Jarnot, R. F., Knosp, B. W., and Lay, R. R.: Earth Observing System (EOS) Aura Microwave Limb Sounder (MLS) Version 5.0x Level 2 and 3 Data Quality and Description Document, Tech. rep., Jet Propulsion Laboratory, California Institute of Technology, Pasadena, California, 68–82, 2022.

Maycock, A. C., Shine, K. P., and Joshi, M. M.: The temperature response to stratospheric water vapour changes, Q. J. Roy. Meteorol. Soc., 137, 1070–1082, 2011.

Millan, L., Santee, M. L., Lambert, A., Livesey, N. J., Werner, F., Schwartz, M. J., Pumphrey, H. C., Manney, G. L., Wang, Y., Su, H., Wu, L., Read, W. G., and Froidevaux, L.: The Hunga Tonga-Hunga Ha'apai hydration of the stratosphere, Geophys. Res. Lett., 49, e2022GL099381, https://doi.org/10.1029/2022GL099381, 2022.

Muller, S. C., Murk, A., Monstein, C., and Kampfer, N.: Intercomparison of digital fast Fourier transform and acoustooptical spectrometers for microwave radiometry of the atmosphere, IEEE T. Geosci. Remote, 47, 2233–2239, 2009.

NASA Jet Propulsion Laboratory: Microwave Limb Sounder, https://mls.jpl.nasa.gov/ (last access: 2 May 2024), 2024.

Nedoluha, G. E., Michael Gomez, R., Allen, D. R., Lambert, A., Boone, C., and Stiller, G.: Variations in middle atmospheric water vapor from 2004 to 2013, J. Geophys. Res.-Atmos., 118, 11285–11293, 2013.

Nedoluha, G. E., Gomez, R. M., Boyd, I., Neal, H., Allen, D. R., Siskind, D. E., Lambert, A., and Livesey, N. J.: Measurements of mesospheric water vapor from 1992 to 2021 at three stations from the Network for the Detection of Atmospheric Composition Change, J. Geophys. Res.-Atmos., 127, e2022JD037227, https://doi.org/10.1029/2022JD037227, 2022.

Nedoluha, G. E., Gomez, R. M., Boyd, I., Neal, H., Allen, D. R., Lambert, A., and Livesey, N. J.: Measurements of stratospheric water vapor at Mauna Loa and the effect of the Hunga

Tonga eruption, J. Geophys. Res.-Atmos., 128, e2022JD038100, https://doi.org/10.1029/2022JD038100, 2023.

Nedoluha, G. E., Gomez, R. M., Boyd, I., Neal, H., Allen, D. R., and Lambert, A.: The spread of the Hunga Tonga H$_2$O plume in the middle atmosphere over the first two years since eruption, J. Geophys. Res.-Atmos., 129, e2024JD040907, https://doi.org/10.1029/2024JD040907, 2024.

Oyj, V.: RS41-SG and RS41-SGP User Guide, Vaisala Oyj, Vanha Nurmijärventie 21, FI-01670 Vantaa, Finland, version M211667EN-H, https://www.vaisala.com (last access: 1 December 2022), 2022.

Rodgers, C. D.: Inverse methods for atmospheric sounding: theory and practice, Vol. 2, World Scientific, https://doi.org/10.1142/3171, 2000.

Sauvageat, E.: Calibration routine for ground-based passive microwave radiometer: a user guide, Tech. rep., University of Bern, Institute of Applied Physics, 2021-01-MW, 39 pp., https://doi.org/10.48350/164418, 2021.

Sauvageat, E., Albers, R., Kotiranta, M., Hocke, K., Gomez, R. M., Nedoluha, G. E., and Murk, A.: Comparison of three high resolution real-time spectrometers for microwave ozone profiling instruments, IEEE J. Sel. Top. Appl., 14, 10045–10056, 2021.

Sauvageat, E., Maillard Barras, E., Hocke, K., Haefele, A., and Murk, A.: Harmonized retrieval of middle atmospheric ozone from two microwave radiometers in Switzerland, Atmos. Meas. Tech., 15, 6395–6417, https://doi.org/10.5194/amt-15-6395-2022, 2022.

Schranz, F., Tschanz, B., Rüfenacht, R., Hocke, K., Palm, M., and Kämpfer, N.: Investigation of Arctic middle-atmospheric dynamics using 3 years of H$_2$O and O$_3$ measurements from microwave radiometers at Ny-Ålesund, Atmos. Chem. Phys., 19, 9927–9947, https://doi.org/10.5194/acp-19-9927-2019, 2019.

Virtanen, P., Gommers, R., Oliphant, T. E., Haberland, M., Reddy, T., Cournapeau, D., Burovski, E., Peterson, P., Weckesser, W., Bright, J., van der Walt, S. J., Brett, M., Wilson, J., Millman, K. J., Mayorov, N., Nelson, A. R. J., Jones, E., Kern, R., Larson, E., Carey, C J., Polat, İ., Feng, Y., Moore, E. W., VanderPlas, J., Laxalde, D., Perktold, J., Cimrman, R., Henriksen, I., Quintero, E. A., Harris, Charles R., Archibald, A. M., Ribeiro, A. H., Pedregosa, F., van Mulbregt, P., and SciPy 1.0 Contributors: SciPy 1.0: Fundamental Algorithms for Scientific Computing in Python, Nat. Methods, 17, 261–272, https://doi.org/10.1038/s41592-019-0686-2, 2020.

Shi, G., Krochin, W., Sauvageat, E., and Stober, G.: Ozone and water vapor variability in the polar middle atmosphere observed with ground-based microwave radiometers, Atmos. Chem. Phys., 23, 9137–9159, https://doi.org/10.5194/acp-23-9137-2023, 2023.

Sica, R. J. and Haefele, A.: Retrieval of water vapor mixing ratio from a multiple channel Raman-scatter lidar using an optimal estimation method, Appl. Optics, 55, 763–777, https://doi.org/10.1364/AO.55.000763, 2016.

Solomon, S., Rosenlof, K. H., Portmann, R. W., Daniel, J. S., Davis, S. M., Sanford, T. J., and Plattner, G.-K.: Contributions of stratospheric water vapor to decadal changes in the rate of global warming, Science, 327, 1219–1223, 2010.

Straub, C., Tschanz, B., Hocke, K., Kämpfer, N., and Smith, A. K.: Transport of mesospheric H$_2$O during and after the stratospheric sudden warming of January 2010: observation and simulation, Atmos. Chem. Phys., 12, 5413–5427, https://doi.org/10.5194/acp-12-5413-2012, 2012.

Thölix, L., Karpechko, A., Backman, L., and Kivi, R.: Linking uncertainty in simulated Arctic ozone loss to uncertainties in modelled tropical stratospheric water vapour, Atmos. Chem. Phys., 18, 15047–15067, https://doi.org/10.5194/acp-18-15047-2018, 2018.

Verdes, C., Bühler, S., von Engeln, A., Kuhn, T., Künzi, K., Eriksson, P., and Sinnhuber, B.-M.: Pointing and temperature retrieval from millimeter-submillimeter limb soundings, J. Geophys. Res.-Atmos., 107, ACH 10-1–ACH 10-24, 2002.

Waters, J. W., Froidevaux, L., Harwood, R. S., Jarnot, R. F., Pickett, H. M., Read, W. G., Siegel, P. H., Cofield, R. E., Filipiak, M. J., Flower, D. A., Holden, J. R., Lau, G. K., Livesey, N. J., Manney, G. L., Pumphrey, H. C., Santee, M. L., Wu, D. L., Cuddy, D. T., Lay, R. R., Loo, M. S., Perun, V. S., Schwartz, M. J., Stek, P. C., Thurstans, R. P., Boyles, M. A., Chandra, K. M., Chavez, M. C., Gun-Shing Chen and Chudasama, B. V., Dodge, R., Fuller, R. A., Girard, M. A., Jiang, J. H., Jiang, Y., Knosp, B. W., LaBelle, R. C., Lam, J. C., Lee, K. A., Miller, D., Oswald, J. E., Patel, N. C., Pukala, D. M., Quintero, O., Scaff, D. M., Van Snyder, W., Tope, M. C., Wagner, P. A., and Walch, M. J.: The earth observing system microwave limb sounder (EOS MLS) on the Aura satellite, IEEE T. Geosci. Remote, 44, 1075–1092, https://doi.org/10.1109/TGRS.2006.873771, 2006.

Zhou, X., Dhomse, S. S., Feng, W., Mann, G., Heddell, S., Pumphrey, H., Kerridge, B. J., Latter, B., Siddans, R., Ventress, L., Querel, R., Smale, P., Asher, E., Hall, E. G., Bekki, S., and Chipperfield, M. P.: Antarctic vortex dehydration in 2023 as a substantial removal pathway for Hunga Tonga-Hunga Ha'apai water vapor, Geophys. Res. Lett., 51, e2023GL107630, https://doi.org/10.1029/2023GL107630, 2024.